Continuous Functionally Graded Material to Improve the Thermoelectric Properties of ZnO

Corson Cramer[a], Jesus Gonzalez-Julian[b], Paul Colasuonno[a], and Troy Holland[a],

a Advanced Materials Processing and Testing Lab, Colorado State University, 80523 Fort Collins, CO, USA

b Institute of Energy and Climate Research, IEK-1, Materials Synthesis and Processing, Forschungszentrum, Jülich, 52425 Jülich, Germany

Abstract

Functionally graded material (FGM) in terms of grain size gradation is fabricated from ZnO with a combination of modified Spark Plasma Sintering (SPS) graphite tooling, water sintering enhancements through transient liquid phase surface transport, and strategic SPS mechanical loading. The grain size gradation of the ZnO FGM is an order of magnitude across a 10 mm thick, fully dense sample. This is the first semiconductor or ceramic to be graded microstructurally to this extent. Predictions of the microstructure with a Master Sintering Curve (MSC) approach were done with a series of isothermal experiments on two different FGM conditions revealing a slight offset due to a constrained mechanism. The mechanical properties were tested with Vickers micro hardness across the sample, showing a gradient in hardness. In addition, the thermoelectric properties of the FGM were measured and show an enhancement of the zT at lower temperature by an order of magnitude compared to uniform small- and large-grained samples making a new path for improvements of bulk thermoelectric material.

Introduction

Transient heat sources are seeking thermoelectric generators (TEGs) with wider temperature bandwidth to capture more waste heat in a larger temperature range [1]. TEGs with segmentation improvements as well as well as homogenous property manipulation have shown to improve efficiency in bulk material, and bulk material is of interest due to higher currents allowed versus thin films [2], [3] [4], [5]. FGM is one way to improve the efficiency and useful temperature range of thermoelectrics, and TEGs based on carrier concentration manipulation have improved the efficiency by 8-12 % and improved the useful temperature range in some studies, yet no method of fabricating a continuous material has been created until now [6], [7]. Work started on FGM thermoelectrics in terms of segmentation, carrier concentration, and microstructure was proposed in some work [1], and it is shown that the grain size has a large effect on the thermoelectric properties [8] [9]. A study on small, large, and randomly mixed grain size thermoelectric samples showed that small grains had the best performance [10]. Spark plasma sintering (SPS) techniques have already been explored to fabricate FGMs with modified tooling [11]. A conical die arrangement is used to induce an in-situ thermal gradient during the sintering in order to densify different phases of material at different spots in the die axially [12]. One group created an axial microstructural gradient from fully dense to open porosity in a single step by using an offset die arrangement [13]. The concept of an offset die is used in another study to stabilize phase and create the first grain size gradient in an axial sample [14]. The first SPS process for specifically FGM TEGs was designed with the conical die approach and is intended for microstructural variation [15]. A layered powder system with different dopant concentrations was fabricated using a free sintering method and was tested with $Pb_{1-x}Sn_xTe$ but was not compared to homogenous samples [16].

Zinc oxide (ZnO) is a good candidate for microelectronic and high temperature thermoelectric devices because the electrical conductivity is enhanced in pure nanocrystalline ZnO caused by interstitial Zn and oxygen vacancies, and the Seebeck at elevated temperatures remains high [17][18][19]. It is a good

model material to use for thermoelectrics because it is abundant, safe, cost efficient, and relatively easy to process. Some SPS work on ZnO showed that with sintering aids the temperature at which it sinters can be reduced to 400°C [20], [21]. It was later shown that the compaction plays a key role, and the presence of acetate phase is necessary to achieve sintering at this low of temperature [22]. Also SPS studies have also shown that the heating rate plays a significant role in sintering when trying to sinter zinc oxide at lower temperature [23], [24]. The largest improvement in sintering ZnO was done by adding 1.5 monolayers of deionized water on the surface of the ZnO by injection into the compacted green body. The water is thought to help the densification in four major ways; the first is improved initial packing density due to less friction between particles, the second is a purposed hydroxide ion mass transport, the third is a liquid phase surface transport of the Zn and O ions, and the fourth is a surface cleaning that consumes the carbonate that would inhibit mass transport [25][26].

In this research, a novel approach to thermoelectric improvement targets a large microstructural transition using ZnO as a model material. This is done in one step to create a continuous microstructural gradient. Rather than making a graded composition or phase, a continuous gradation of grain size is achieved in a 10 mm thick ZnO sample by modifying the SPS tooling and using water as a transient liquid phase. In order to capture a large range of microstructure, the sintering at lower temperatures was previously optimized [25], and the higher temperature sintering has to contribute to grain growth of fully dense material. With a Master Sinter Curve (MSC) approach [27], the effects of various heating rates and temperatures on the sintering of ZnO can be used to help understand and predict the microstructure with a series of isothermal experiments. The microstructural gradient is a brand new method for improving the figure of merit for a thermoelectric device (zT), and this is the first time it has been done. The zT for many ZnO systems including doped polycrystalline ZnO has been in the range of 10^{-5} to 10^{-2} in the temperature range of 100°C to 400°C, which already makes our pure ZnO competitive with what is currently used [19], [28], [29]. In terms of FGM TEGs, this is the first ceramic and semiconductor material to be fabricated with grain size gradation of an order of magnitude in a continuous sample. Making sintered FGM ZnO in terms of grain size allows for better controllability of properties and tunability for higher efficiency thermoelectrics, varistors, and piezo electrics.

Procedure

Sintering

Commercially available ZnO nanopowder (US Research Nanomaterials, Inc.) with high purity of 99.95 % and average particle size of 18 nm was used in these studies. A Scanning Electron Microscope (SEM) image and an X-ray diffraction (XRD) pattern of the ZnO powder are shown below in Figure 1. The particle size is verified with SEM and XRD using the Williamson-Hall method [30].

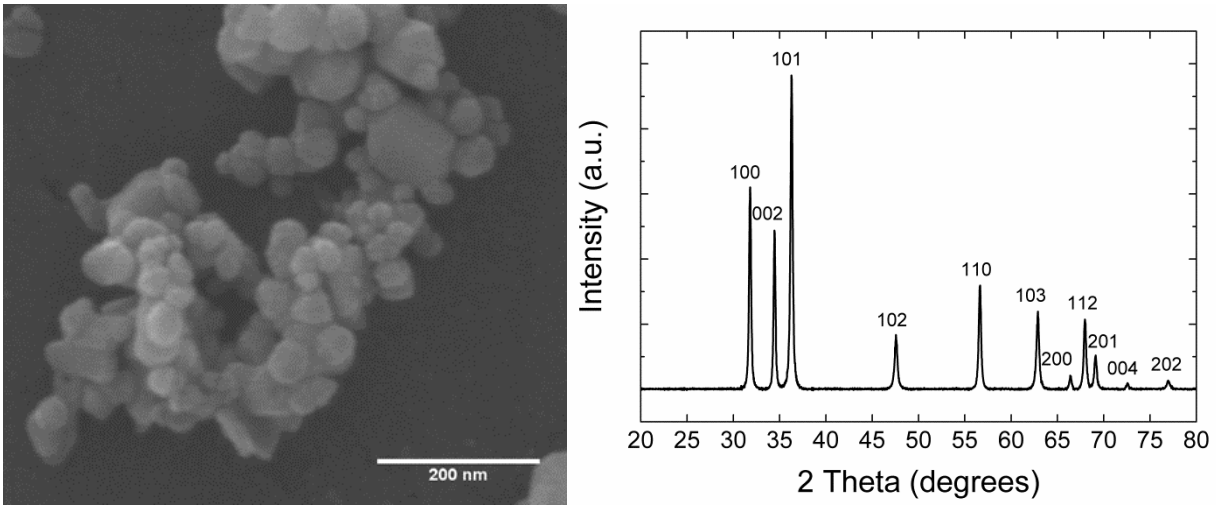

Figure 1: ZnO powder from US Research Nanomaterials, Inc. (US Nano). SEM image (left) and XRD pattern (right).

Prior to sintering, the powder was stored in a desiccator for up to 72 hours. One hour prior to sintering, the powder is exposed to atmosphere as it transferred to a fume hood for loading. 18 g is weighed out and loaded into a die of 20 mm inner diameter with graphite foil around the circumference. The sintering setup is pressed in the SPS (Fuji Dr. Sinter) at 16 MPa for 1 minute in air in order to get a green body. The setup is taken out and 200 microliters of deionized water is injected with a micropipette into each side of the green compact, a piece of graphite foil is placed on top of the powder, the plunger faces are sprayed with BN spray to ensure that no field effects are present, and the plungers are re-inserted. The sintering setup is then placed back into the SPS for 5 minutes at 32 MPa to homogenously distribute the water into the powder by means of capillary action. The sintering setup is then loaded with top and bottom thermocouples so that they are 2 mm away from the powder.

The approach for predictions is to achieve faster sintering versus slower sintering conditions and then try to achieve these same conditions spatially in one setup. In order to predict the microstructure of a continuously graded sample, isothermal samples are sintered with a typical SPS graphite die setup in order to understand and predict the density and grain size evolution over time using an MSC approach. Three different heating schedules (175°C/min to 900°C, 125°C/min to 700°C, and 75°C/min to 500°C) are run isothermally controlling from the plunger of a typical SPS sintering setup and added to one plot to show the predictive behavior. The sintering for the three heating schedules is cut off at 97% dense, ½ the hold time, and the full hold time. This gives a density-grain size-time (DGT) plot of conditions that can predict the final microstructure of system with differential heating schedules. Two DGT plots are made for two different mechanical load schedules because of a large water outgassing. One load schedule starts with high load (73 MPa) during the low temperature bake out and is released right before the large water outgassing to 35 MPa, and the other starts with low load (35 MPa) during the low temperature bake out and is increased to 73 MPa after the large water outgassing. The loads are controlled at 0.1 kN per second.

In order to achieve the different heating schedules from the DGT spatially in one sintering setup, a novel sintering setup is made to achieve differential sintering. In this approach, one plunger has less contacting area to the die and thus has higher current density as shown in Figure 2. This creates a local hot spot on that side and a temperature field or thermal gradient (TG) across the sintering specimen. The heating schedules from the DGT are matched spots spatially in the TG specimen. For TG sintering, the material

near the hot side will densify more quickly and start grain growth, while the material on the other side will densify more slowly due to lower temperature. This differential sintering across the sample results in a continuously graded microstructure in terms of grain size or even porosity. The SPS setup for the thermal gradient (TG) sintering is shown below in Figure 2. There is an alumina sleeve to aid in mechanical support and insulation of the hot side graphite punch, BN spray is used around the hot side punch for more insulation, and an external graphite sleeve is used for more support and a heat sink. BN is also sprayed on the plunger faces to achieve higher thermal gradient and negate the effects of electric field. All of these modifications are necessary to get the maximum temperature gradient across the sintering sample. The TG is controlled from the hot side plunger and the cold side temperature is monitored to understand the total temperature gradient and heating rates within the TG system. For the two mechanical loads, the efficacy of the DGT plot is evaluated for how well it can predict a thermal gradient system's microstructure.

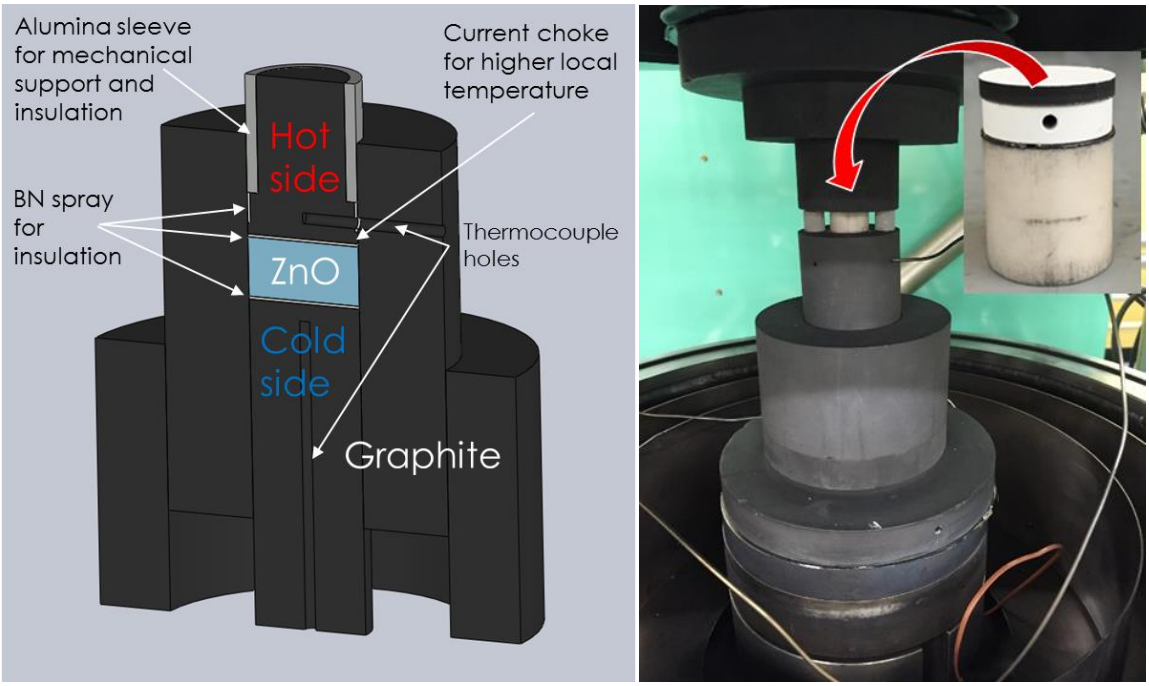

Figure 2: 3-D representation of the whole sintering setup (left) and fully machined sintering setup used in thermal gradient sintering (right).

SEM images are taken of the microstructure to find the grain size and understand the microstructure of the thermal gradient sample versus the isothermal predictive samples. Image analysis using fracture surfaces and the intercept procedure (ASTM E112, [31]) with a correction factor of 1.56 was performed to determine the grain size, and histograms are made for thermal gradient and isothermal samples. Densities were first measured geometrically, verified with the Archimedes method, and checked for areal density in samples with varying density. Vickers Micro hardness is done on a fully dense FGM sample at a load of 9.8 kgf and dwell time of 15 seconds taking 6 indentations at every location tested. Thermoelectric properties including Seebeck coefficient, electrical resistivity, and thermal conductivity were measured as a function of temperature up to 400°C on the fully dense FGM and compared to samples of small grains and large grains. The Seebeck coefficient and resistivity were measured with the Kohlrausch method where sections are 2 x 2 x 10 mm sections [32], [33], and the thermal conductivity is measured using a modified transient plane method with geometry of the final sintered specimens [34]–

[36]. All samples measured for electrical and thermal properties were calcined after sintering to ensure defects are at an equilibrium state for all samples.

Results and Discussion

Isothermal Predictive Sintering

Isothermal sintering is done for three heating schedules, 175°C/min to 900°C, 125°C/min to 700°C, and 75°C/min to 500°C, and a mechanical load starting at 35 MPa and increasing to 75 MPa after a large water outgassing in order to gain a predictive model for the microstructure of the FGM ZnO. This DGT predicts a fully dense system where the grain size is an average of 1.8 micrometers on one side and 250 nm on the other.

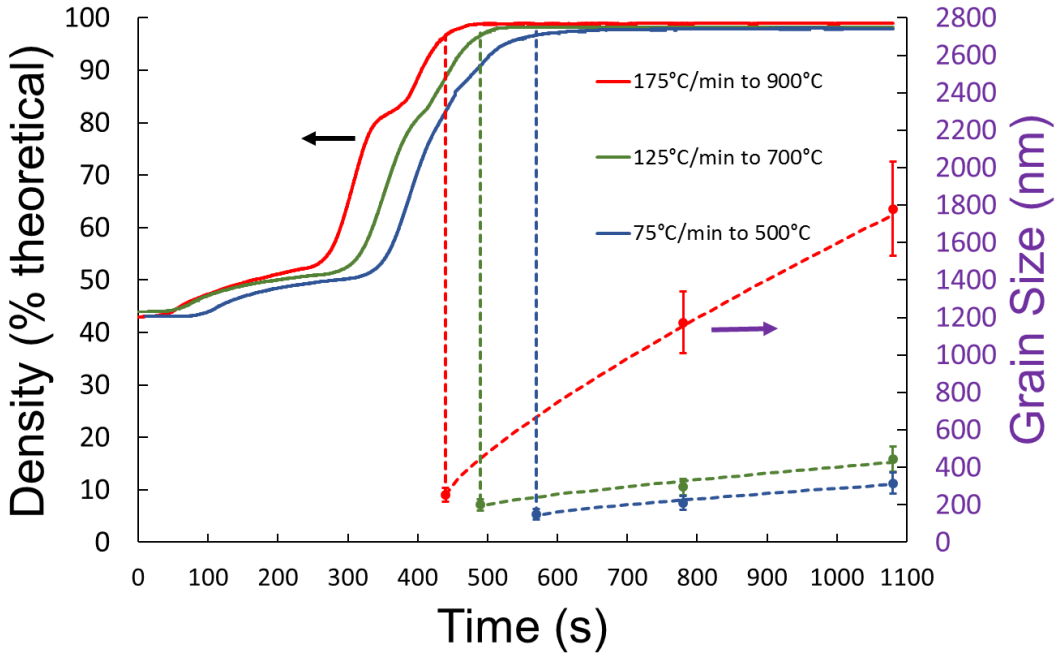

Figure 3: DGT plot for microstructural prediction of continuous sample done when load is ramped to 73 MPa after large water outgassing.

A second DGT is done with a different load schedule. This DGT is done to gain more information about the TG sintering system and predict different conditions that can be processed in a TG sample. In this DGT, the predicted microstructure is a fully dense side with some noticeable grain growth to a continuously more porous side. This shows that the pressure affects this system significantly, and that fully dense samples will need enough mechanical load to achieve full density. The difference in the two DGT systems is about 30 MPa.

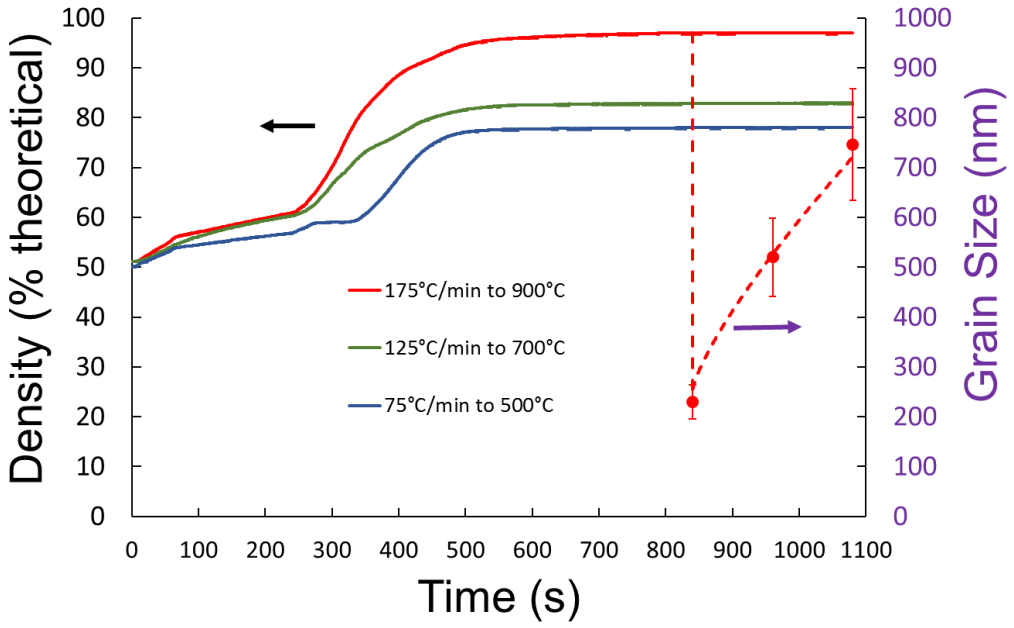

Figure 4: DGT plot for microstructural prediction of continuous sample done when load is decreased to 35 MPa before the large water outgassing.

Thermal Gradient Sintering

The temperature and vacuum schedule for the thermal gradient samples is shown in Figure 5. The temperature of the hot side control point (175°C/min to 900°C) and the cold side (75°C/min to 500°C) in the TG sample are measured and are very close to the DGT heating schedules for the 175°C/min to 900°C and 75°C/min to 500°C, but some iterative action was done to achieve this because of the mechanical load schedule as varying the load in SPS is not a common practice but was found necessary to allow the large amount of water to outgas. The temperature of the geometric middle in the TG samples are assumed to be an average of the hot and cold side temperatures at 125°C/min to 700°C. Nevertheless, the heating rates and hold temperatures in Figure 5 are spatially recreated in one sintering specimen using the modified tooling setup from Figure 2.

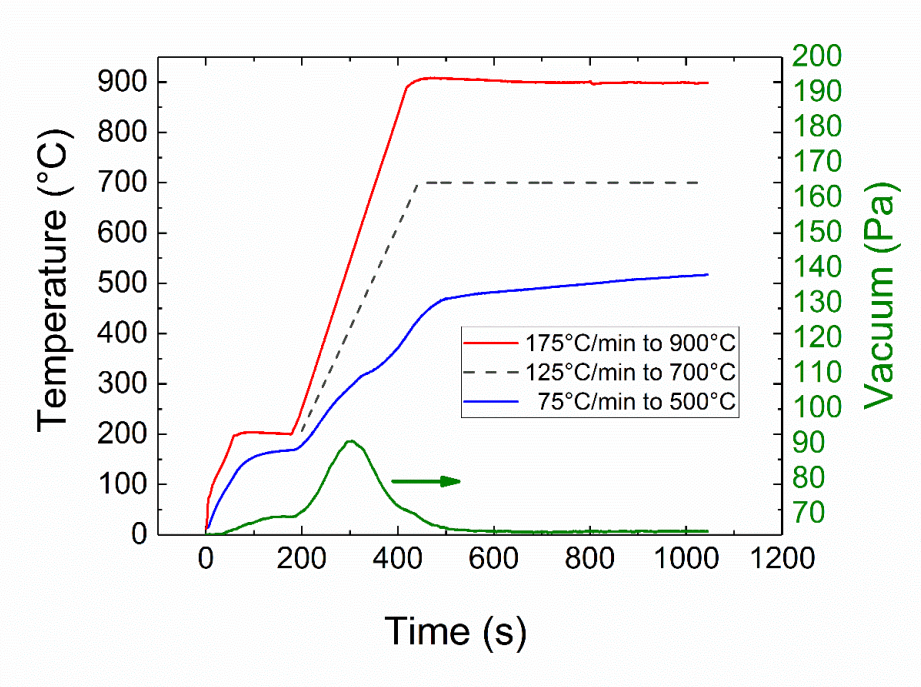

Figure 5: Temperature data collected from thermal gradient sintering sample done when load is ramped to 73 MPa after the large water outgassing.

The two TG samples are compared in the table below. It shows, that when dropping the load before outgassing, the sample cannot reach full density. Load has a profound effect on the system, and a sufficient amount is needed to close pores and keep densification as the favorable mechanism in a wide range of sintering temperatures. The TG sample where load is applied after the large water outgassing reaches full density.

Table 1: Comparison of thermal gradient sintering conditions and density.

	2wt% injected water	
Load during initial bake out	35	73
Load after large water outgassing (MPa)	73	35
Density of TG Sample (% theoretical)	98	86

The TG sample that was sintered to full density can be seen below. A macro- and microscopic view of the material is shown. It is seen that the sample is not noticeably reduced to non-stoichiometric ZnO by retaining its yellowish/white color, is fully dense, and has a large microstructural gradient across the sample. There was no notable grain size gradient radially.

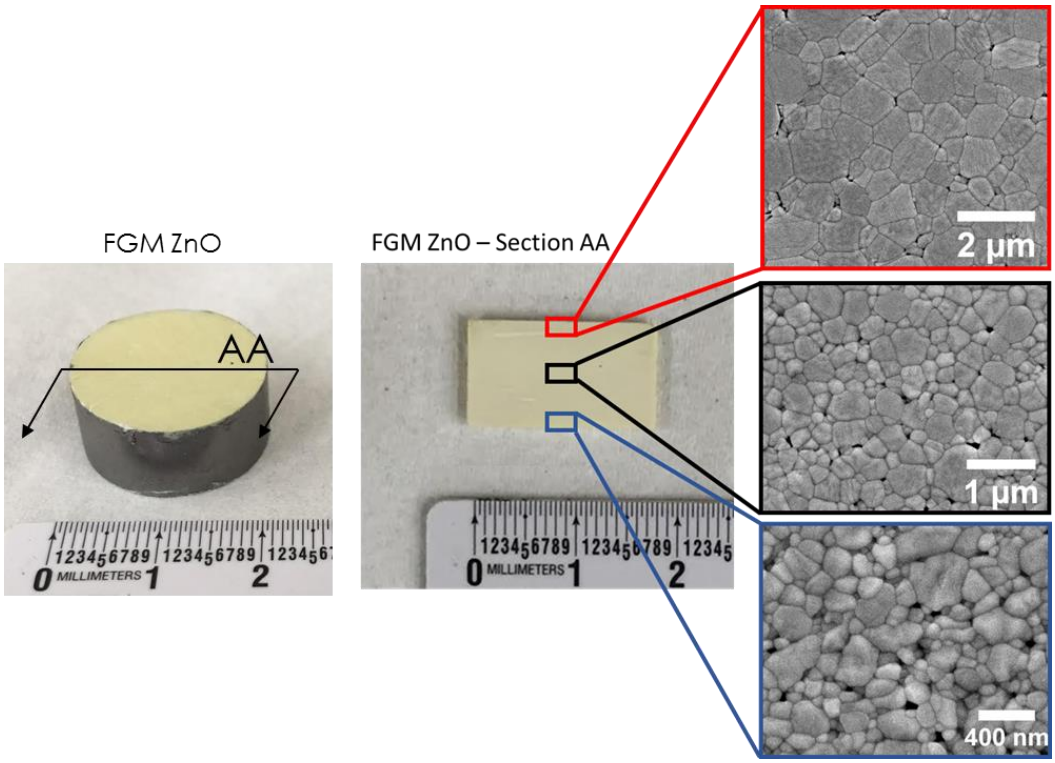

Figure 6: Macroscopic cross section and microscopic images of fully dense FGM ZnO.

The grain size gradation plot of the fully dense TG sample can be seen in Figure 7, and it follows a decaying exponential because each mm increment is representative of a different temperature, and temperature is known to affect the grain growth exponentially [37]–[39]. The achieved grain size gradation is close to an order of magnitude, which should have an influence on the electrical, thermal, and mechanical properties along the axial direction of the FGM [40]. Others have achieved small changes in microstructure targeting different phases [12] [13] [14], but this is the first semiconductor or ceramic to be graded microstructurally to this extent. No one has made a continuous grain size gradation in 10 mm of material with close to an order of magnitude grain size difference.

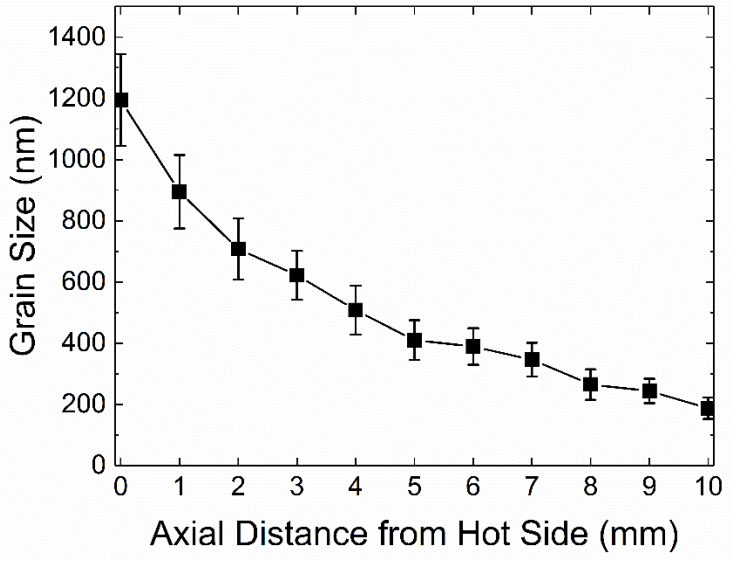

Figure 7: Grain size gradation of fully dense thermal gradient sample.

Microstructural Comparison of thermal gradient system vs. isothermal predictions

The microstructure of spatial locations in the thermal gradient are compared to their direct isothermal predictions. For the first load schedule, the comparison is shown in **Error! Reference source not found.**, and it is clear that the isothermal microstructure predictions are different than the thermal gradient sample. The grain sizes in the isothermal predictions are larger than those at the corresponding location in the thermal gradient at each condition yielding evidence of a constrained system in the thermal gradient sintering system.

Table 2: Comparison of ending grain size for thermal gradient sample versus isothermal predictions done when load is ramped to 73 MPa after the large water outgassing.

Isothermal Predictions (DGT)		Thermal Gradient (FGM)	
Condition	End Grain Size (nm)	Condition	Grain Size (nm)
175°C/min to 900°C	1781 ± 617	175°C/min to 900°C	1194 ± 430
125°C/min to 700°C	436 ± 125	125°C/min to 700°C	389 ± 133
75°C/min to 500°C	316 ± 96	75°C/min to 500°C	187 ± 98

A look at the grain size and distribution of the TG versus the isothermal predictions can be seen below, and the two show a large distribution of grain sizes and a clear difference in the average grain size due to a constraint on the system. The morphology and pore locations are very similar showing little differences in the sintering conditions.

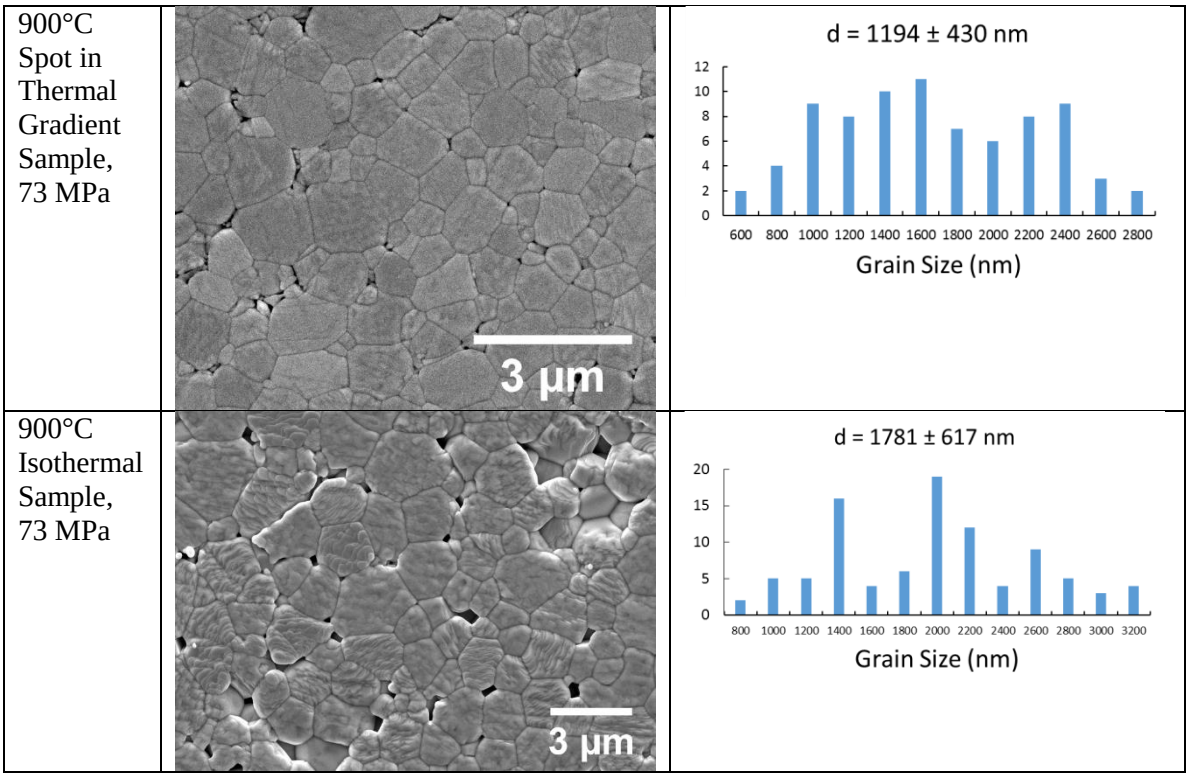

Figure 8: Microstructural comparisons for TG versus isothermal predictions based on grain size and distribution for the system when load is ramped to 73 MPa after the large water outgassing.

The DGT done with less mechanical load during the high temperature hold yielded a prediction that is not fully dense, and the TG sample is made to compare the sintering. The TG sample follows the same trend as the DGT but is again under estimating the microstructure because the grain size on the hot side is smaller than the isothermal prediction and the density on the cold side is lower than the predicted isothermal sample giving more evidence of a constrained system. This shows that with another load there is evidence of a constraint. Also, mechanical load plays a significant role in sintering the ZnO FGM system. The image of the macro to microstructure is shown below, and a table is made to compare to the isothermal predictions of the microstructure at the end of the high temperature hold.

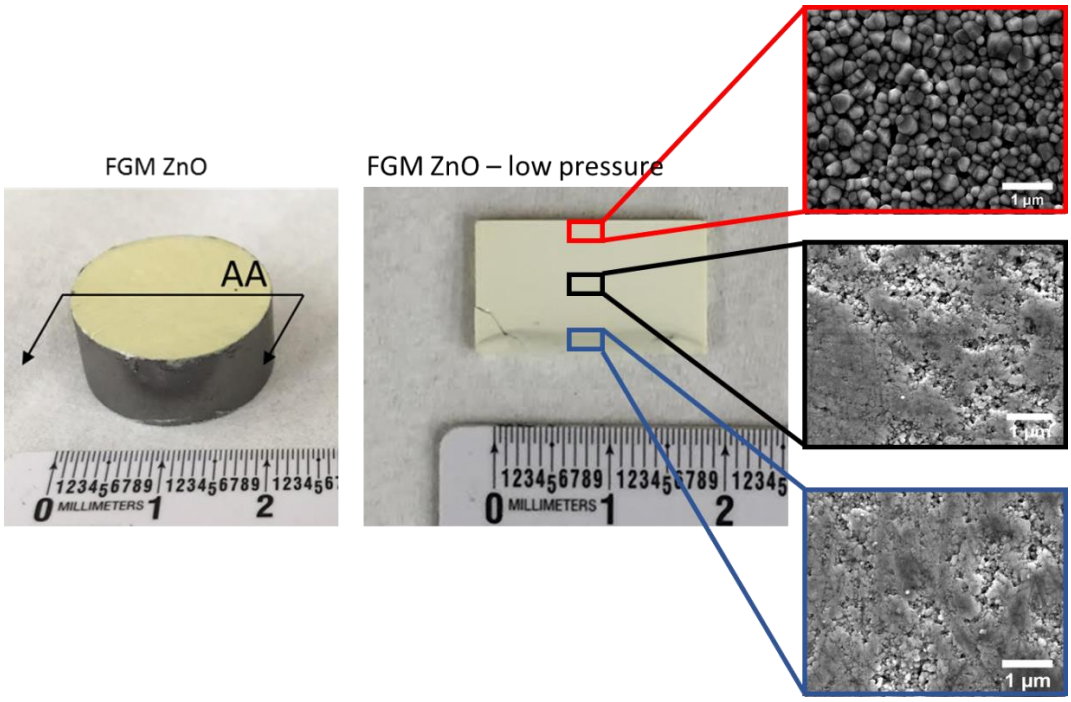

Figure 9: Macro- and microstructural image of TG sample done when the load is decreased to 35 MPa before the large water outgassing.

Table 3: Comparison of ending grain size or density for thermal gradient sample versus isothermal predictions done when load is released to 35 MPa before the large water outgassing.

Isothermal Predictions (DGT)		Thermal Gradient (FGM)	
Condition	End Grain Size (nm)	Condition	End Grain Size (nm)
175°C/min to 900°C	750 ± 273, 98%	175°C/min to 900°C	397 ± 146, 98%
125°C/min to 700°C	83%	125°C/min to 700°C	80%
75°C/min to 500°C	78%	75°C/min to 500°C	76%

This purposed constrained behavior arises from the that fact that at any time during sintering there is a large thermal gradient along the material which causes different densification and thus strain rates as seen in Figure 3 and Figure 4. The higher temperature sinters more quickly and will have closed porosity sooner than the underlying material at less temperature causing the stress states to change continuously along the porosity or microstructural gradient. This creates a pressure shielding of the underlying material and impedes the colder side densification because it is not exposed to the same load distribution and stress states as the hotter side with less porosity. The effects of different stress states on ceramic sintering is explored in Bordia and Raj [41]. The stress states have been known to affect the densification of a porous body by affecting the diffusion paths [42]. In our case the stress states at the colder side most likely retard diffusion mechanism yielding a less developed microstructure than isothermal predictions that have the same stress state throughout the sample. Initial evidence of this hindrance is the smaller grain sizes in the TG sample compared to its isothermal prediction at three different spots. The amount of pressure to overcome this could be calculated, and it is estimated form our work and one previous study to be between 19 MPa and 30 MPa [25].

Micro Hardness Data on Fully Dense FGM

Typical values for the hardness of ZnO are in the range of 1-2.5 GPa for grain sizes varying from 2-5 micrometers [43]. This lower value of hardness lines up with our hot side of the sample which has grain size of about 1.2 micrometers. The side with smaller grains has improved hardness, and the decrease in grain size shows an increase in hardness showing a Hall-Petch-like relationship [44]–[46]. This relationship is because smaller grains have smaller and less cracks of critical length. This fabrication method provides a designable FGM other than thermoelectrics that could be used for thermal shock purposes, cutting tools, and piezoelectrics.

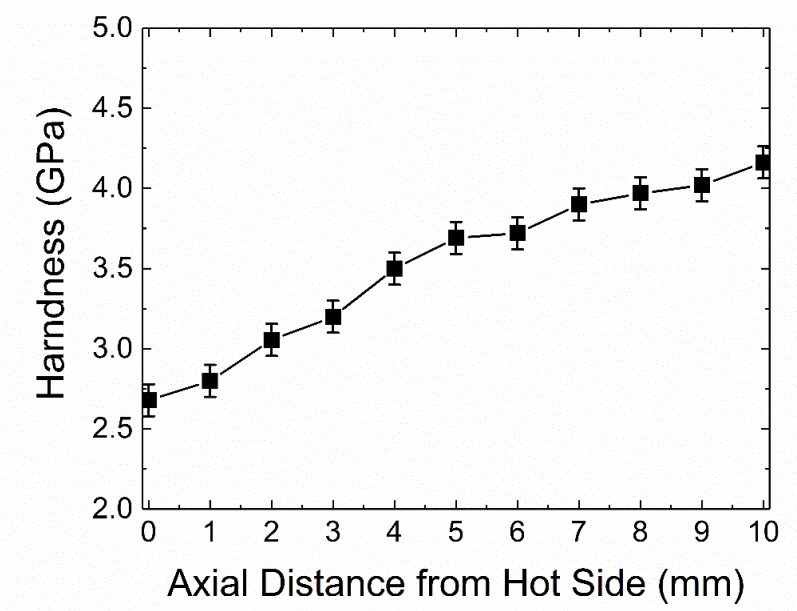

Figure 10: Vickers Micro Hardness axial traverse down the fully dense FGM ZnO.

TEG Properties on Fully Dense FGM

Knowledge of the higher load DGT allows for samples to be made with grain sizes that are comparable to the hot and cold side of the TG sample in order to compare the FGM to a large- and small-grained sample for a direct comparison of TEG properties versus microstructure as shown in Figure 11. The small-grained sample has grain size of 200 nm ± 30 nm and is associated with the cold side processing, and the large grained sample has grain size of 1250 nm ± 240 nm and is associated with the hot side processing. The FGM is tested with heat flow in both directions, and no differences were noted in properties except with thermal conductivity. Thermal conductivity of the FGM is higher when the heat flux is exposed to the large-grained side as opposed to the small-grained side.

It is evident that this microstructural gradation affects the FGM Seebeck coefficient because at lower temperatures, the Seebeck coefficient is closer to the small-grained sample value and at higher temperatures, the Seebeck coefficient is closer to the large-grained sample value. The FGM resistivity and thermal conductivity behave more like the large-grained sample at all temperatures. The small-grained sample has the highest zT at temperature. The large-grained sample has a similar trend in zT as the small-grained sample but is less in magnitude. The trends in thermoelectric properties of the small-grained and large-grained samples is in accord with many studies done on grain size effects [8], [10], [47]. The FGM

has an order of magnitude higher zT at lower temperature compared to the small- and large-grained samples, and the FGM has lower zT at higher temperature.

The tail-end of the zT is improved in our system. Because the Seebeck coefficient transitions from a value near the small-grained sample value at lower temperature to a value closer to the large-grained at higher temperature shows initial evidence of an enhanced system and a compensation of the thermoelectric voltage. The resistivity of the FGM is slightly better than the large-grained sample, so it should have Seebeck that is less than that of the large-grained sample [48]. The fact that the Seebeck coefficient of the FGM has not depleted is more evidence of a Seebeck coefficient enhancement along the sample. This enhancement of the zT temperature range is similar to the one proposed in Jin et al. where the properties are optimized for given locations in the material based on the temperature to maximize the current density [49]. It has also been shown that there is an averaging effect with the Seebeck of segmented TEGs similar to the effect demonstrated in this research because the current density will change across the sample depending on the grain size, but the FMG will remain higher than the large-grained uniform sample because of the location of the small grains near the hot side of the TEG material. This Seebeck coefficient enhancer renders an apparent Seebeck coefficient in the FGM [50]. It is also confirmed that the resistivity can vary and be less in magnitude in the FGM than in uniform samples like the phenomenon seen in this study [51]. Another reason for enhanced resistivity in the FGM can be attributed to the thermal gradient sintering process and contact resistance and adherence. Since the samples are calcined after SPS, the only effects from defects should be due to grain size effects solely. The enhancements do not seem to resemble a dopant FGM system [1]. The enhancements are also very similar to segmented systems, but the studies done have not done a full thermoelectric property study, so it is unclear if the properties are additive in an FGM [52]–[55].

The ZnO FGM is able to improve the zT by an order of magnitude at the lower temperatures tested. We have successfully made a path for improving thermoelectric temperature range with ZnO as a candidate material and a model process using the grain size as the variable. This method is not optimized but shows that this a new method for improving thermoelectrics. Since the effects are prevalent in ZnO, this method should in theory work on any bulk thermoelectric material. Also, our system should provide higher efficiency compared to a segmented TEG because there is no contact resistance between segments as the gradation is continuous, but no direct comparison has been done yet.

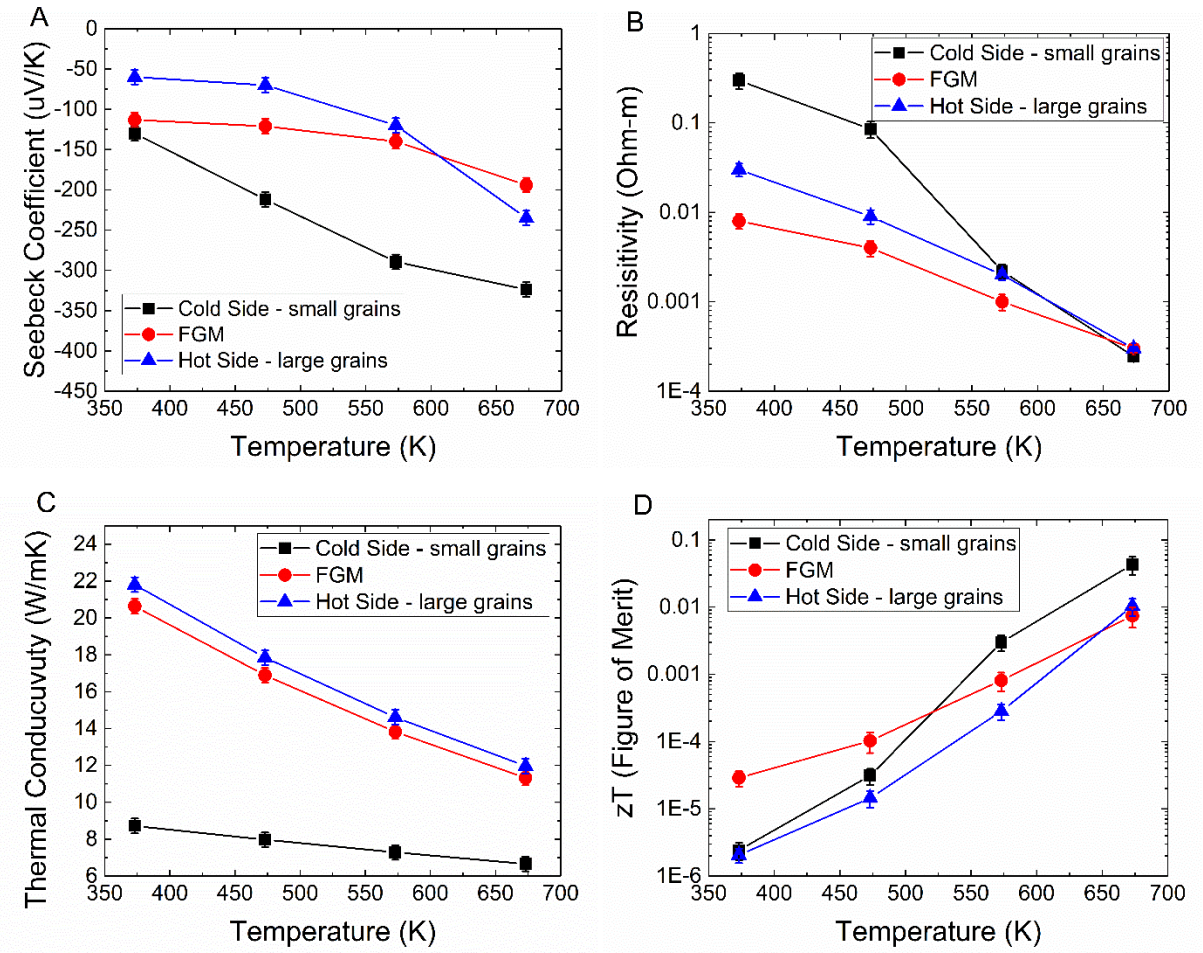

Figure 11: Thermoelectric properties of the fully dense thermal gradient sample versus isothermal samples with the same size grains as the extremes seen in the thermal gradient sample. (a) Seebeck and (b) resistivity, and (c) thermal conductivity are measured, and the zT (d) is calculated.

Conclusion

We are able to fabricate a continuous sample in one step with a grain size gradation of almost an order of magnitude in a 10 mm span of material using modified tooling, transient water assisted sintering, and strategic loads with commercially available material. The maximum temperature on the plunger of 900°C is not enough to reduce the material. The grain size gradation follows an exponential decay along the axial direction. There is constrained sintering in the thermal gradient system which inhibits the final grain growth to be less than the predicted DGT model done with isothermal predictions. It is apparent that load plays a significant role in the FGM ZnO system in order for a wide range of sintering temperatures to reach full density because the grain growth and density are less than predicted with DGTs for two different applied mechanical loads. The mechanical properties show a gradation along the sample that could benefit many micromechanical systems. Lastly, the thermoelectric properties show an enhanced zT temperature bandwidth with an order of magnitude improvement at lower temperature by mechanisms of property gradient. This is a new method for improving bulk thermoelectric material and can be applied to many other materials.

References

[1] M. Koizumi, “FGM activities in Japan,” *Compos. Part B Eng.*, vol. 28, no. 1–2, pp. 1–4, 1997.

[2] J. Schilz, L. Helmers, W. E. Müller, and M. Niino, “A local selection criterion for the composition of graded thermoelectric generators,” *J. Appl. Phys.*, vol. 83, no. 2, pp. 1150–1152, Jan. 1998.

[3] E. Müller, Č. Drašar, J. Schilz, and W. A. Kaysser, “Functionally graded materials for sensor and energy applications,” *Mater. Sci. Eng. A*, vol. 362, no. 1–2, pp. 17–39, Dec. 2003.

[4] O. Yamashita, S. Tomiyoshi, and K. Makita, “Bismuth telluride compounds with high thermoelectric figures of merit,” *J. Appl. Phys.*, vol. 93, no. 1, pp. 368–374, Jan. 2003.

[5] S. Ohta, T. Nomura, H. Ohta, and K. Koumoto, “High-temperature carrier transport and thermoelectric properties of heavily La- or Nb-doped SrTiO3 single crystals,” *J. Appl. Phys.*, vol. 97, no. 3, p. 034106, Feb. 2005.

[6] A. E. Kaliazin, V. L. Kuznetsov, and D. M. Rowe, “Rigorous calculations related to functionally graded and segmented thermoelements,” in *XX International Conference on Thermoelectrics, 2001. Proceedings ICT 2001*, 2001, pp. 286–292.

[7] Z. Dashevsky, Y. Gelbstein, I. Edry, I. Drabkin, and M. P. Dariel, “Optimization of thermoelectric efficiency in graded materials,” in *Thermoelectrics, 2003 Twenty-Second International Conference on - ICT*, 2003, pp. 421–424.

[8] K. Kishimoto and T. Koyanagi, “Preparation of sintered degenerate n-type PbTe with a small grain size and its thermoelectric properties,” *J. Appl. Phys.*, vol. 92, no. 5, pp. 2544–2549, Sep. 2002.

[9] Y. Gao, Y. He, and L. Zhu, “Impact of grain size on the Seebeck coefficient of bulk polycrystalline thermoelectric materials,” *Chin. Sci. Bull.*, vol. 55, no. 1, pp. 16–21, Jan. 2010.

[10] L.-D. Zhao, B.-P. Zhang, W.-S. Liu, and J.-F. Li, “Effect of mixed grain sizes on thermoelectric performance of Bi2Te3 compound,” *J. Appl. Phys.*, vol. 105, no. 2, p. 023704, Jan. 2009.

[11] D. Giuntini, J. Raethel, M. Herrmann, A. Michaelis, and E. A. Olevsky, “Advancement of Tooling for Spark Plasma Sintering,” *J. Am. Ceram. Soc.*, vol. 98, no. 11, pp. 3529–3537, Nov. 2015.

[12] C.-Q. Hong, X.-H. Zhang, W.-J. Li, J.-C. Han, and S.-H. Meng, “A novel functionally graded material in the ZrB2–SiC and ZrO2 system by spark plasma sintering,” *Mater. Sci. Eng. A*, vol. 498, no. 1–2, pp. 437–441, Dec. 2008.

[13] D. M. Hulbert, D. Jiang, U. Anselmi-Tamburini, C. Unuvar, and A. K. Mukherjee, “Continuous functionally graded boron carbide-aluminum nanocomposites by spark plasma sintering,” *Mater. Sci. Eng. A*, vol. 493, no. 1–2, pp. 251–255, Oct. 2008.

[14] M. Belmonte, J. Gonzalez-Julian, P. Miranzo, and M. I. Osendi, “Continuous in situ functionally graded silicon nitride materials,” *Acta Mater.*, vol. 57, no. 9, pp. 2607–2612, May 2009.

[15] L. P. Bulat *et al.*, “On fabrication of functionally graded thermoelectric materials by spark plasma sintering,” *Tech. Phys. Lett.*, vol. 40, no. 11, pp. 972–975, Dec. 2014.

[16] Y. Gelbstein, Z. Dashevsky, and M. P. Dariel, “Powder metallurgical processing of functionally graded p-Pb1−xSnxTe materials for thermoelectric applications,” *Phys. B Condens. Matter*, vol. 391, no. 2, pp. 256–265, Apr. 2007.

[17] C.-W. Nahm, “Nonohmic properties of V/Mn/Nb/Gd co-doped zinc oxide semiconducting varistors with low-temperature sintering process,” *Mater. Sci. Semicond. Process.*, vol. 23, pp. 58–62, Jul. 2014.

[18] R. N. Viswanath, S. Ramasamy, R. Ramamoorthy, P. Jayavel, and T. Nagarajan, “Preparation and characterization of nanocrystalline ZnO based materials for varistor applications,” *Nanostructured Mater.*, vol. 6, no. 5–8, pp. 993–996, 1995.

[19] K. H. Kim, S. H. Shim, K. B. Shim, K. Niihara, and J. Hojo, “Microstructural and Thermoelectric Characteristics of Zinc Oxide-Based Thermoelectric Materials Fabricated Using a Spark Plasma Sintering Process,” *J. Am. Ceram. Soc.*, vol. 88, no. 3, pp. 628–632, Mar. 2005.

[20] J. G.-J. Benjamin Dargatz, “Effect of electric field and atmosphere on the processing of nanocrystalline ZnO,” *Proc. SPIE - Int. Soc. Opt. Eng.*, vol. 8987, 2014.
[21] S. Schwarz, A. M. Thron, J. Rufner, K. Benthem, and O. Guillon, “Low Temperature Sintering of Nanocrystalline Zinc Oxide: Effect of Heating Rate Achieved by Field Assisted Sintering/Spark Plasma Sintering,” *J. Am. Ceram. Soc.*, vol. 95, no. 8, pp. 2451–2457, Aug. 2012.
[22] J. G.-J. Benjamin Dargatz, “Improved compaction of ZnO nano-powder triggered by the presence of acetate and its effect on sintering,” *Sci. Technol. Adv. Mater.*, vol. 16, no. 2, p. 025008, 2015.
[23] L. Gao, Q. Li, W. Luan, H. Kawaoka, T. Sekino, and K. Niihara, “Preparation and Electric Properties of Dense Nanocrystalline Zinc Oxide Ceramics,” *J. Am. Ceram. Soc.*, vol. 85, no. 4, pp. 1016–1018, Apr. 2002.
[24] J. Wang and L. Gao, “Photoluminescence Properties of Nanocrystalline ZnO Ceramics Prepared by Pressureless Sintering and Spark Plasma Sintering,” *J. Am. Ceram. Soc.*, vol. 88, no. 6, pp. 1637–1639, Jun. 2005.
[25] B. Dargatz *et al.*, “FAST/SPS sintering of nanocrystalline zinc oxide—Part I: Enhanced densification and formation of hydrogen-related defects in presence of adsorbed water,” *J. Eur. Ceram. Soc.*
[26] B. Dargatz, J. Gonzalez-Julian, M. Bram, Y. Shinoda, F. Wakai, and O. Guillon, “FAST/SPS sintering of nanocrystalline zinc oxide—Part II: Abnormal grain growth, texture and grain anisotropy,” *J. Eur. Ceram. Soc.*
[27] H. Su and D. L. Johnson, “Master Sintering Curve: A Practical Approach to Sintering,” *J. Am. Ceram. Soc.*, vol. 79, no. 12, pp. 3211–3217, 1996.
[28] Y. Kinemuchi, M. Mikami, K. Kobayashi, K. Watari, and Y. Hotta, “Thermoelectric Properties of Nanograined ZnO,” *J. Electron. Mater.*, vol. 39, no. 9, pp. 2059–2063, Dec. 2009.
[29] S. Walia *et al.*, “Transition metal oxides – Thermoelectric properties,” *Prog. Mater. Sci.*, vol. 58, no. 8, pp. 1443–1489, Oct. 2013.
[30] G. K. Williamson and W. H. Hall, “X-ray line broadening from filed aluminium and wolfram,” *Acta Metall.*, vol. 1, no. 1, pp. 22–31, Jan. 1953.
[31] “Standard Test Methods for Determining Average Grain Size - Google Search.” [Online]. Available: https://www.google.com/search?q=Standard+Test+Methods+for+Determining+Average+Grain+Size&rlz=1C1CHBD_enUS701US701&oq=Standard+Test+Methods+for+Determining+Average+Grain+Size&aqs=chrome..69i57j69i60&sourceid=chrome&ie=UTF-8. [Accessed: 04-Oct-2016].
[32] H. G. Jensen, “Kohlrausch Heat Conductivity Apparatus for Intermediate or Advanced Laboratory,” *Am. J. Phys.*, vol. 38, no. 7, pp. 870–874, Jul. 1970.
[33] B. M. Gol’tsman and M. G. Komissarchik, “Measurement of thermal and electrical conductivities of small cross section samples in the 80–400 °K range,” *J. Eng. Phys.*, vol. 20, no. 3, pp. 385–389, Mar. 1971.
[34] S. A. Al-Ajlan, “Measurements of thermal properties of insulation materials by using transient plane source technique,” *Appl. Therm. Eng.*, vol. 26, no. 17–18, pp. 2184–2191, Dec. 2006.
[35] C. DIXON, M. R. STRONG, and S. M. ZHANG, “Transient Plane Source technique for measuring thermal properties of silicone materials used in electronic assemblies,” *Int. J. Microcircuits Electron. Packag.*, vol. 23, no. 4, pp. 494–500, 2000.
[36] S. E. Gustafsson, “Transient plane source techniques for thermal conductivity and thermal diffusivity measurements of solid materials,” *Rev. Sci. Instrum.*, vol. 62, no. 3, pp. 797–804, Mar. 1991.
[37] D. V. Quach, H. Avila-Paredes, S. Kim, M. Martin, and Z. A. Munir, “Pressure effects and grain growth kinetics in the consolidation of nanostructured fully stabilized zirconia by pulsed electric current sintering,” *Acta Mater.*, vol. 58, no. 15, pp. 5022–5030, 2010.

[38] R. M. German, “Coarsening in Sintering: Grain Shape Distribution, Grain Size Distribution, and Grain Growth Kinetics in Solid-Pore Systems,” *Crit. Rev. Solid State Mater. Sci.*, vol. 35, no. 4, pp. 263–305, Nov. 2010.
[39] J. Narayan, “Grain growth model for electric field-assisted processing and flash sintering of materials,” *Scr. Mater.*, vol. 68, no. 10, pp. 785–788, May 2013.
[40] Y. Zhao, Y. Yan, A. Kumar, H. Wang, W. D. Porter, and S. Priya, “Thermal conductivity of self-assembled nano-structured ZnO bulk ceramics,” *J. Appl. Phys.*, vol. 112, no. 3, p. 034313, Aug. 2012.
[41] R. k. Bordia and R. Raj, “Sintering Behavior of Ceramic Films Constrained by a Rigid Substrate,” *J. Am. Ceram. Soc.*, vol. 68, no. 6, pp. 287–292, Jun. 1985.
[42] R. K. Bordia and G. W. Scherer, “On constrained sintering—I. Constitutive model for a sintering body,” *Acta Metall.*, vol. 36, no. 9, pp. 2393–2397, 1988.
[43] T. K. Roy, “Assessing hardness and fracture toughness in sintered zinc oxide ceramics through indentation technique,” *Mater. Sci. Eng. A*, vol. 640, pp. 267–274, Jul. 2015.
[44] R. W. Rice, C. C. Wu, and F. Boichelt, “Hardness–Grain-Size Relations in Ceramics,” *J. Am. Ceram. Soc.*, vol. 77, no. 10, pp. 2539–2553, Oct. 1994.
[45] N. Hansen, “Hall–Petch relation and boundary strengthening,” *Scr. Mater.*, vol. 51, no. 8, pp. 801–806, Oct. 2004.
[46] J. A. Wollmershauser *et al.*, “An extended hardness limit in bulk nanoceramics,” *Acta Mater.*, vol. 69, pp. 9–16, May 2014.
[47] M. Takashiri, K. Miyazaki, S. Tanaka, J. Kurosaki, D. Nagai, and H. Tsukamoto, “Effect of grain size on thermoelectric properties of n-type nanocrystalline bismuth-telluride based thin films,” *J. Appl. Phys.*, vol. 104, no. 8, p. 084302, Oct. 2008.
[48] “Thermoelectrics Handbook: Macro to Nano,” *CRC Press*, 09-Dec-2005. [Online]. Available: https://www.crcpress.com/Thermoelectrics-Handbook-Macro-to-Nano/Rowe/p/book/9780849322648. [Accessed: 02-Jan-2017].
[49] Z.-H. Jin and T. T. Wallace, “Functionally Graded Thermoelectric Materials with Arbitrary Property Gradations: A One-Dimensional Semianalytical Study,” *J. Electron. Mater.*, vol. 44, no. 6, pp. 1444–1449, Jun. 2015.
[50] L. N. Vikhor and L. I. Anatychuk, “Generator modules of segmented thermoelements,” *Energy Convers. Manag.*, vol. 50, no. 9, pp. 2366–2372, Sep. 2009.
[51] J. L. Cui, X. B. Zhao, W. M. Zhao, and Y. P. Lu, “Preparation, thermoelectric properties and interface analysis of n-type graded material FeSi2/Bi2Te3,” *Mater. Sci. Eng. B*, vol. 94, no. 2–3, pp. 223–228, Jun. 2002.
[52] M. S. El-Genk and H. H. Saber, “High efficiency segmented thermoelectric unicouple for operation between 973 and 300 K,” *Energy Convers. Manag.*, vol. 44, no. 7, pp. 1069–1088, May 2003.
[53] M. S. El-Genk, H. H. Saber, and T. Caillat, “A performance comparison of SiGe and skutterudite based segmented thermoelectric devices,” in *AIP Conference Proceedings*, 2002, vol. 608, pp. 1007–1015.
[54] P. H. Ngan *et al.*, “Towards high efficiency segmented thermoelectric unicouples,” *Phys. Status Solidi A*, vol. 211, no. 1, pp. 9–17, Jan. 2014.
[55] T. T. Wallace, Z.-H. Jin, and J. Su, “Efficiency of a Sandwiched Thermoelectric Material with a Graded Interlayer and Temperature-Dependent Properties,” *J. Electron. Mater.*, vol. 45, no. 4, pp. 2142–2149, Feb. 2016.